

Chapter 8

Modified Hopkinson Apparatus to Investigate Fluid Cavitation as a Potential Source of Injury

Michael Bustamante, Dilaver Singh, and Duane S. Cronin

Abstract Mild Traumatic Brain Injury (mTBI) has been recognized as an important issue for persons exposed to blast. Specifically, this injury has been associated with exposure to blast overpressure and more recently relatively large negative pressures have been identified as occurring at the posterior regions of the brain in experimental and in numerical studies of frontal blast exposure. These negative pressures are caused by the reflection of the incident bar stress wave from the free surface of the skull, and may be intensified due to focusing effects from the curvature of the skull. Under certain circumstances, this negative pressure is hypothesized to cause cavitation of cerebrospinal fluid (CSF) surrounding the brain, potentially resulting in injury to the brain. Unfortunately the cavitation pressure of CSF has not been directly measured, so the consequence of negative pressures in numerical head models exposed to blast cannot be accurately predicted. The cavitation pressure of fluids is highly variable, depending on the presence of impurities in the fluid and the presence of dissolved gasses. In this study, a modified Compressive Split Hopkinson Pressure Bar (CSHPB) apparatus incorporating a sealed confinement chamber was used to generate negative pressures in distilled water to investigate the cavitation properties of water as a surrogate for CSF. The negative pressures in the fluid were measured using a pressure transducer designed for compression and validated in comparison to the input signal on the modified Hopkinson bar apparatus, as well as verified by a numerical model of the experiment. The CSHPB apparatus was used to generate initial compressive waves ranging from 1.85 to 7.85 MPa to produce cavitation in distilled water. The experimental tests were simulated with good agreement and used to obtain water peak negative pressures ranging from -1.32 to -5.64 MPa. Future tests will be undertaken to investigate cavitation properties of CSF.

Keywords Cavitation • Split Hopkinson pressure bar • Mild traumatic brain injury • Negative pressure • Impedance mismatch

8.1 Introduction

Mild Traumatic Brain Injury (mTBI) has become an increasingly important and prevalent issue for persons exposed to blast. The United States Department of Defence defines mTBI as a head injury that results in alteration or loss of consciousness [1]. In the last decade, blast events in theatre account for up to 80 % of the TBI experienced by US service members, of which approximately 75 % are classified as mTBI [1]. Currently, mTBI is diagnosed through clinical assessment with functional deficits and neurological tests [2]. Service members that are exposed to non-physically-impairing injury from blasts are evaluated to determine their ability to return to duty [1]. These assessments and evaluations are based on approaches used to address sports concussions, which may not translate well to service members exposed to blast [1].

There are four commonly referenced mechanisms that can cause bodily harm to an individual from blast exposure (Fig. 8.1). The injuries caused by these mechanisms are described as the primary, secondary, tertiary, and quaternary blast injury. Primary blast injury is defined as any injury caused by the initial blast wave created by the rapid expansion of gases during an explosive detonation [3, 4]. This large overpressure generated by a blast, when interacting with the body can produce contusions, lacerations, and herniation of internal organs [4, 5]. Projectiles and debris propelled by the blast that pierce the skin, such as shrapnel, are categorized as secondary blast injury [3, 4]. Tertiary blast injuries occur when the body experiences large accelerations from a blast resulting from whole body translations such as being thrown against a wall, or acceleration of non-penetrating masses towards the body [3–6]. All other injuries, such as chemical, thermal, and nuclear effects of blasts are categorized under quaternary blast injuries [3–6].

M. Bustamante (✉) • D. Singh • D.S. Cronin

Department of Mechanical Engineering, University of Waterloo, 200 University Ave. W., Waterloo, ON, Canada N2L3G1
e-mail: mcbustam@uwaterloo.ca

Fig. 8.1 Blast mechanisms which can cause bodily harm

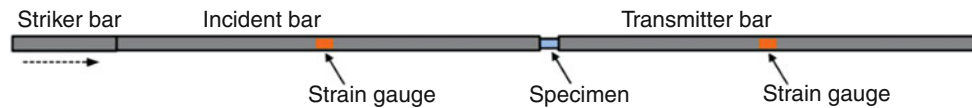
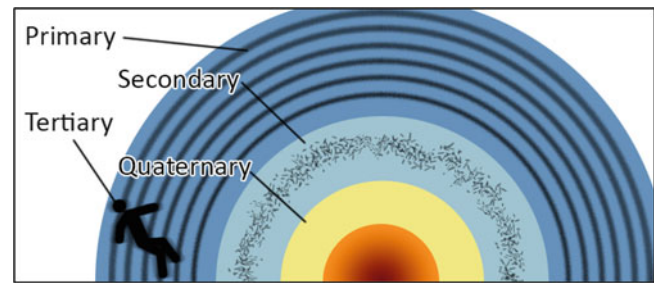


Fig. 8.2 Traditional CSHPB setup consisting of a striker, incident, and transmitter bar of the same material [13]

Due to the ethical concerns of using human *in vivo* measurements of brain response exposed to blast, studies often use animal models or numerical head models to determine the effects of the primary blast wave on the brain. It is hypothesized that cavitation of cerebrospinal fluid (CSF) due to transient negative intracranial pressure is a possible injury mechanism that can lead to mTBI. Cavitation is the generation of voids or cavities (i.e. bubbles) in a liquid due to localized pressure changes. When these bubbles collapse they can create jets of liquid that can produce large forces on surrounding materials [7]. The limits of CSF cavitation are currently unknown and many numerical studies that examine the effects of CSF cavitation in the brain use the cavitation limit of water which ranges from 0.1 to 120 MPa [8]. Published literature has shown that negative pressures can occur in the brain during the initial positive pressure phase of a blast. An experimental study by Bir (2011) measured negative pressures during frontal blast exposure in the parietal and occipital lobe using optical pressure sensors installed in fresh unembalmed post-mortem head surrogates. Negative pressures were noted for all specimens tested and reflected the change in orientation of the blast (i.e. negative pressures occurred at the contrecoup) [8]. A numerical study by Singh et al. (2013) modelled primary blast injury to the head using sagittal and transverse models of the head. These models showed the greatest negative intracranial pressures occurring at the posterior ranging from -211 to -760 kPa for the load cases considered in that study [10]. Panzer et al. (2012) modelled a 2D slice of the head in the transverse plane and assumed a CSF pressure cut-off of -100 kPa which was found to produce cavitation in the model before the negative pressure phase of the blast [11]. Zhang et al. (2013) tested the effects of an Advanced Combat Helmet on the numerical Wayne State University Head Injury Model (WSUHIM), and reported that a 0.35 MPa peak overpressure produced negative pressures ranging from -300 to -480 kPa occurring at the contrecoup [12].

It is hypothesized that the acoustic impedance mismatch between the skull and free surface of the head at the contrecoup may cause the large negative pressures observed in the brain during blast conditions. Due to a higher impedance of the skull compared to the free surface of the head, an incoming compressive wave is reflected as a tensile wave that may cause negative pressures leading to cavitation of CSF. An important property to determine whether cavitation of CSF is an injury mechanism in primary blast is to determine cavitation pressure limits for the CSF. This study will investigate cavitation in distilled water caused by a reflected compressive wave generated by a modified Compressive Split Hopkinson Pressure Bar (CSHPB). A CSHPB is an apparatus that can generate controlled high-rate loading in compression. A traditional CSHPB consists of a striker, incident, and transmitter bar of the same material (Fig. 8.2). When struck by the striker, a compressive wave is generated in the incident bar, travels down the incident bar, through the specimen, and into the transmitter bar.

The compressive wave that is generated in the incident bar is called the incident wave. When the incident wave reaches the incident bar and specimen interface, a portion of the wave is transmitted through the specimen and into the transmitter bar (i.e. the transmitted wave) and the balance of the wave is reflected at the interface and travels back through the incident bar (i.e. the reflected wave) (Fig. 8.3). Analysis of the incident, transmitted, and reflected waves can be used to determine the dynamic behaviour of the specimen. The fraction of the incident wave that is reflected is determined by the impedance mismatch between the bars and specimen (Eqs. 8.1 and 8.2), where σ is stress, ρ is density, C is acoustic waves speed. The product of density and acoustic wave speed is defined as the acoustic impedance of the material. The impedance mismatch between materials also describes the change in sense of the reflected wave when the incident wave travels from a higher to a lower impedance material (Fig. 8.4). This explains how an entire compressive wave is effectively reflected in

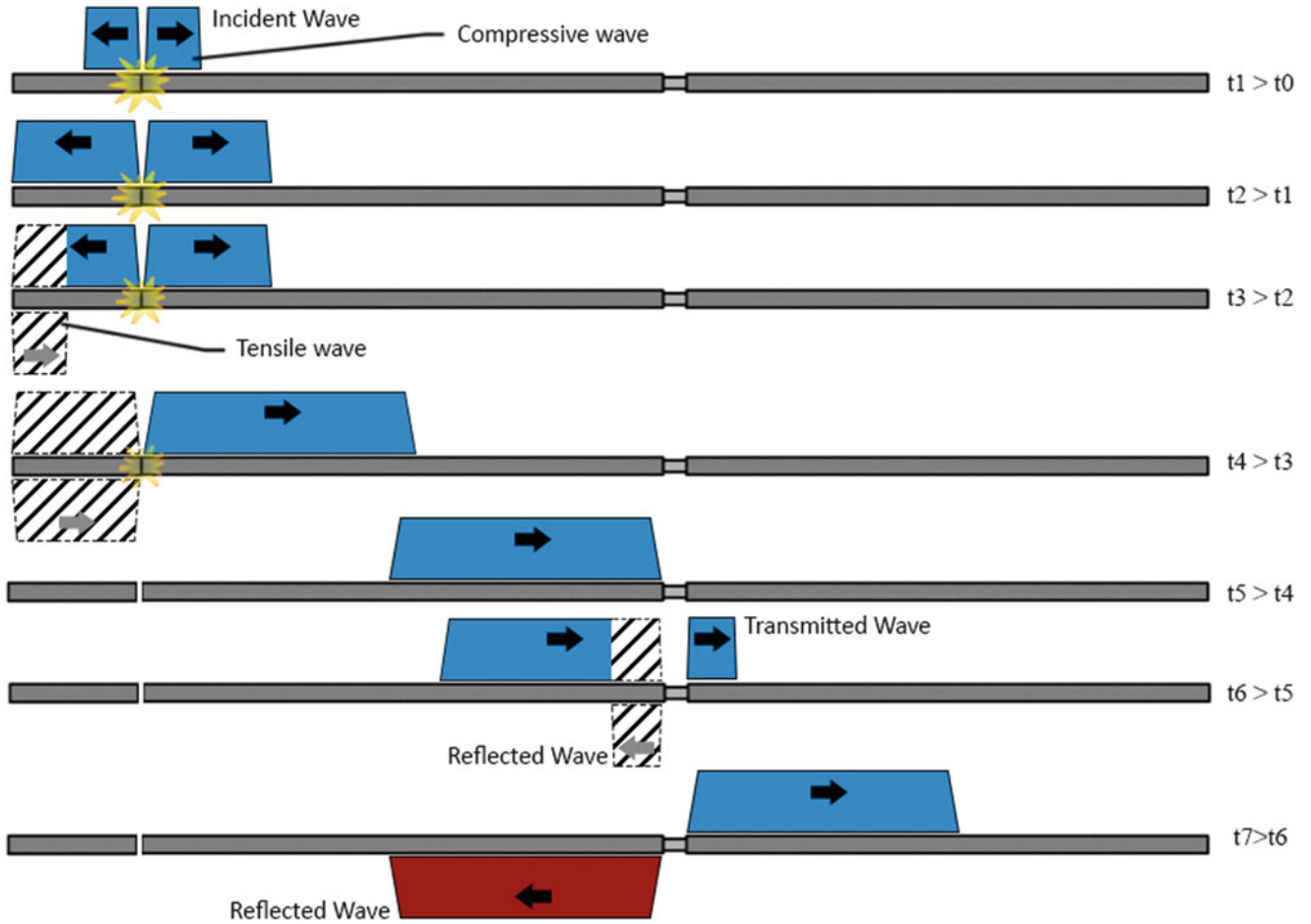


Fig. 8.3 Generation and propagation of incident wave, transmitted wave, and reflected wave in CSHPB after striker impact, where *dashed waves* indicate superposition

tension at the end of a bar, where the adjacent material is of lower impedance (e.g. an aluminum bar end exposed to air, since the impedance of air is far less than that of aluminum).

$$\frac{\sigma_{\text{Reflected}}}{\sigma_{\text{Incident}}} = \frac{(\rho C)_{\text{material}2} - (\rho C)_{\text{material}1}}{(\rho C)_{\text{material}1} + (\rho C)_{\text{material}2}} \quad (8.1)$$

$$\frac{\sigma_{\text{Transmitted}}}{\sigma_{\text{Incident}}} = \frac{2(\rho C)_{\text{material}2}}{(\rho C)_{\text{material}1} + (\rho C)_{\text{material}2}} \quad (8.2)$$

The traditional CSHPB can be altered to a Tensile Split Hopkinson Pressure Bar (TSHPB) that generates an initial tensile wave by replacing the striker bar with a striker tube and affixing an anvil onto the end of the incident bar. The striker tube impacts the anvil generating a tensile wave travelling down the incident bar, through the specimen, and into the transmitter bar. Preliminary tests by Singh et al. (2014) were conducted on a TSHPB apparatus along with a confinement chamber containing distilled water to show cavitation from tensile wave superposition at the interface between the specimen (i.e. distilled water) and transmitter bar (Fig. 8.5) [13]. The TSHPB apparatus was further modified by removing the transmitter bar and replacing the confinement chamber with a single-entry chamber to increase the stiffness of the boundary of interest (Fig. 8.5). A pressure transducer was also mounted flush to the inside wall of the chamber to determine static pressure of the contained water. The modified TSHPB produced cavitation in the distilled water at a negative pressure of approximately -80 kPa from an incident tensile wave with a magnitude of 3.1 MPa. Another similar study by Hong et al. (2014) achieved similar results by producing cavitation in water at a negative pressure of approximately -82 kPa using an initial tensile wave [14]. The pressure transducers used by both Singh and Hong were designed for compression and may not accurately

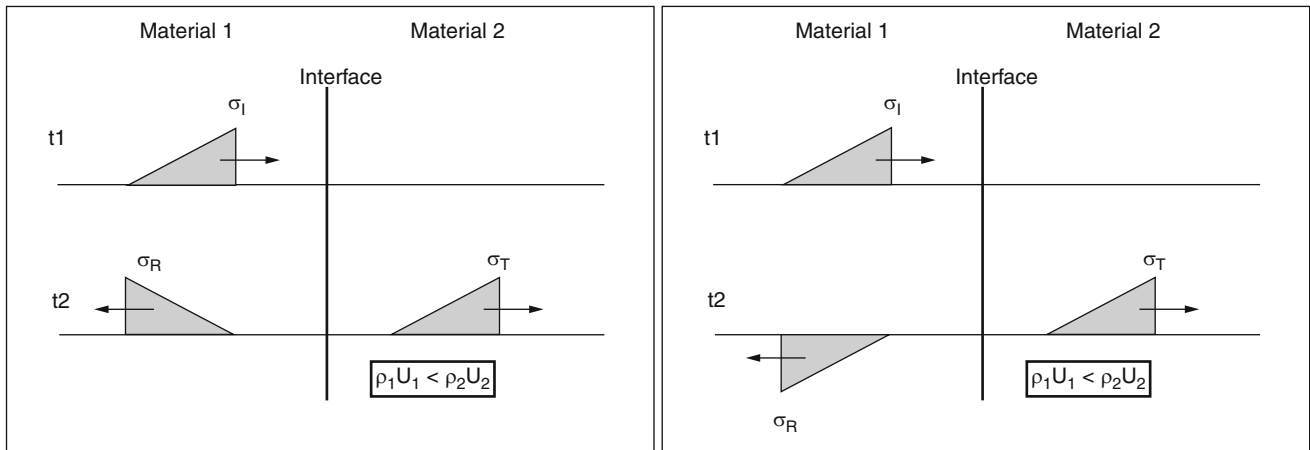


Fig. 8.4 Acoustic impedance difference between two materials, noting the effect on the sense of the reflected wave [16]

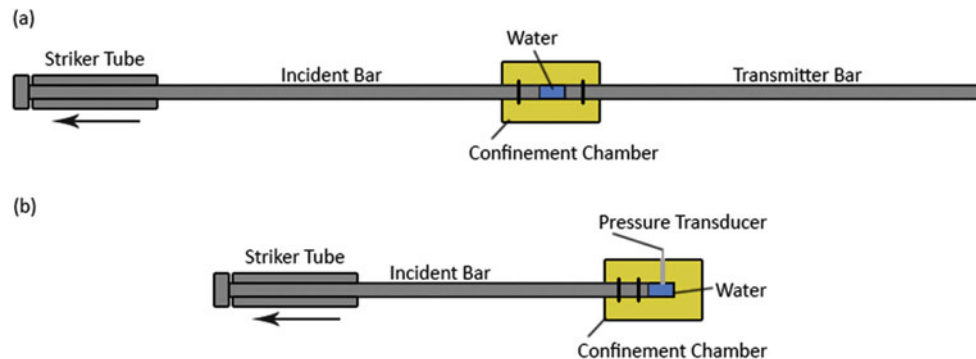


Fig. 8.5 (a) TSHPB setup consisting of a striker tube, incident bar, and transmitter bar of the same material. (b) Modified TSHPB with single-entry confinement chamber

describe the negative pressures in the water. Additionally, these studies used an initial tensile wave rather than an initial compressive wave experienced in blast exposure. In this study a modified CSHPB apparatus was developed to investigate cavitation of distilled water as a result of a reflected compressive wave as hypothesized in blast exposure. The applicability of a pressure transducer designed for compression on measuring negative pressure was also investigated.

8.2 Methods

The experimental setup in this study used a modified CSHPB and an acrylic confinement chamber filled with distilled water (Fig. 8.6). Water was used as a surrogate for CSF, since CSF is primarily water [15, 17]. The striker and incident bar were used to generate a compressive wave that traveled through the water and into the acrylic, and then reflect as a tensile wave at the acrylic and air interface. The CSHPB comprises 25.4 mm diameter aluminum bars with lengths of 2435 and 1068 mm for the incident and striker bars, respectively. The confinement chamber was made of acrylic with an inner diameter of 25.7 mm and an outer diameter of 89 mm. The pressure in the water was measured using a pressure transducer designed for compression (PCB Piezotronics Model 113B21) mounted flush to the inside wall of the chamber. Two o-rings were used to seal the chamber and bar interface to prevent water leakage during tests. A thin layer of dish soap was applied to the inside of the confinement chamber to create a hydrophobic surface to reduce the amount of bubbles developing at the inner wall of the chamber during filling. Distilled water was placed into the chamber through the transducer mount port using a syringe. A syringe was used to minimize the amount of bubbles that would occur if the water were simply poured into the

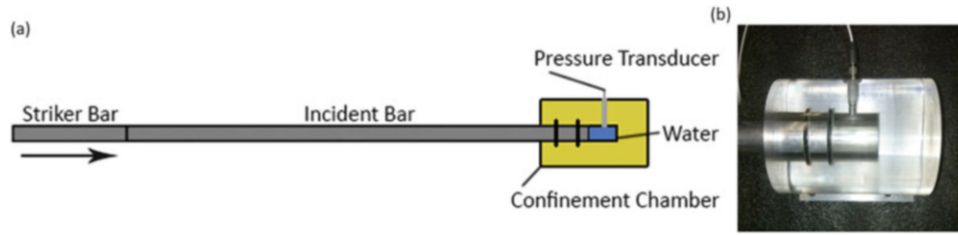


Fig. 8.6 (a) Modified CSHPB with aluminum bars and an acrylic confinement chamber. (b) Photograph of chamber end

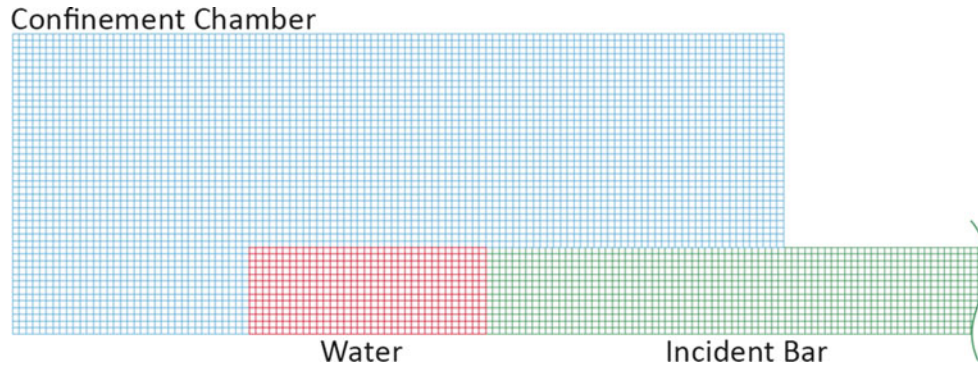


Fig. 8.7 Axisymmetric FE model of experimental CSHPB setup. Striker bar not shown

confinement chamber. Teflon tape was used on the threads of the transducer to seal the chamber. To generate a compressive wave, the striker bar was accelerated to initiate impact with the incident bar. The strain in the bar was measured by strain gages mounted on the incident bar. Measurements are obtained at 2 MHz using LABView 2014 Data Acquisition hardware and software. High-speed imaging of the water was captured at 100,000 fps with a 320×192 resolution.

An axisymmetric model of the experimental test was created using an explicit multi-physics finite element program (LS-DYNA, Version 971 Revision 6.1.1) (Fig. 8.7). The experimental setup was modelled with a total of 50,669 axisymmetric elements. The aluminum bars were modelled as an elastic material with a density of 2700 kg/m^3 , Young's modulus of 68.9 GPa and Poisson's ratio of 0.35. The acrylic chamber was also modelled as an elastic material with a density of 1178 kg/m^3 , Young's modulus of 3.47 GPa and Poisson's ratio of 0.35. The water was modelled as a viscous fluid material with a density of 1000 kg/m^3 and bulk modulus of 2.19 GPa. The interfaces between the incident bar, water, and confinement chamber have incorporated shared nodes since the surfaces were not expected to separate during the simulation time considered. Simulations were performed using striker velocities (V) calculated from Eq. (8.3) where σ is the incident bar stress measured, ρ is the bar density, and C is the bar acoustic wave speed.

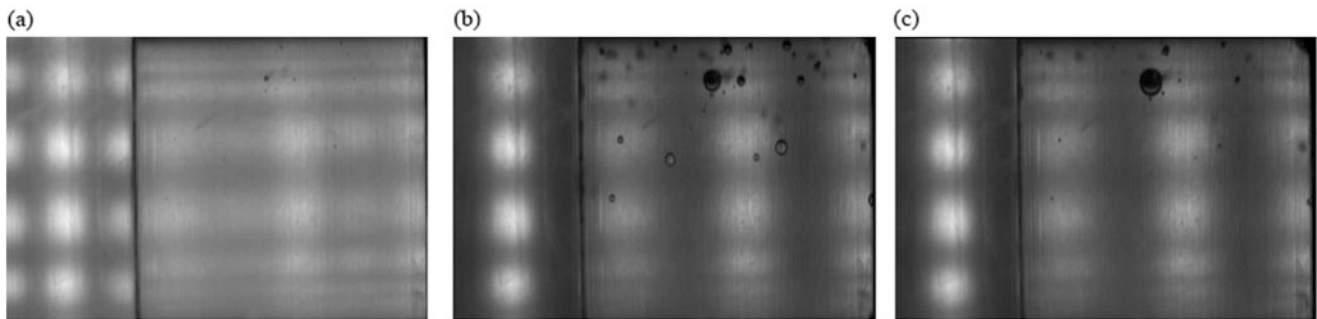
$$\sigma = \frac{1}{2}\rho CV \quad (8.3)$$

8.3 Results

Eight experimental tests were performed with striker velocities ranging from 0.27 to 1.15 m/s resulting in incident bar stress amplitudes ranging from 1.85 to 7.85 MPa, and with peak compressive water pressures ranging from 1.16 to 4.69 MPa (Table 8.1). All tests performed showed cavitation occurring with bubbles developing throughout the volume of the water, with the majority of the bubbles at the interfaces of the water and acrylic and aluminum (Fig. 8.8). Bubbles showed growth and collapse duration of 0.62 ms during the 0.27 m/s impact velocity test. All eight experimental tests were simulated using the striker velocities in Table 8.1. Simulations resulted in incident bar stress amplitudes ranging from 1.86 to 7.88 MPa, positive peak water pressures ranging from 1.27 to 5.38 MPa, and negative peak water pressures ranging from -1.32 to -5.64 MPa (Table 8.2).

Table 8.1 Incident bar stress amplitude, peak water pressure, and calculated striker velocity values for all eight experimental tests

Striker velocity (m/s)	Incident bar stress (MPa)	Peak water pressure (MPa)
0.27	1.85	1.16
0.40	2.75	1.57
0.42	2.88	1.51
0.46	3.12	2.15
0.52	3.58	2.17
0.57	3.90	2.38
1.05	7.17	4.11
1.15	7.85	4.69

**Fig. 8.8** High-speed imaging showing bubble locations and time duration of growth and collapse. (a) Before bubble development. (b) Growth: 0.31 ms. (c) Collapse: 0.62 ms**Table 8.2** Incident bar stress amplitude, positive and negative peak water pressure, and defined striker velocity values for all eight simulations

Striker velocity (m/s)	Incident bar stress (MPa)	Positive peak water pressure (MPa)	Negative peak water pressure (MPa)
0.27	1.86	1.27	-1.32
0.40	2.67	1.88	-1.97
0.42	2.89	1.88	-2.07
0.46	3.13	2.13	-2.24
0.52	3.59	2.44	-2.57
0.57	3.92	2.67	-2.8
1.05	7.19	4.92	-5.16
1.15	7.88	5.38	-5.64

Incident bar stress and water pressure versus time from experimental and numerical data for a striker velocity of 1.15 m/s are compared (Fig. 8.9). Trends of water pressure versus incident bar stress are compared for experimental and numerical data for all test cases performed (Fig. 8.10). Trends of initial water pressure wave (IWPW) versus incident bar stress are compared for experimental, numerical, and analytical data for all test cases performed (Fig. 8.11). The IWPW is the peak pressure measured by the pressure transducer before the first reflection at the water and acrylic interface travels back to the transducer. The analytical data for IWPW was obtained from Eq. (8.2) using experimental incident bar stress values in Table 8.1. The IWPW values of experimental tests are obtained at the same time as the easily visible IWPW values in the numerical simulations.

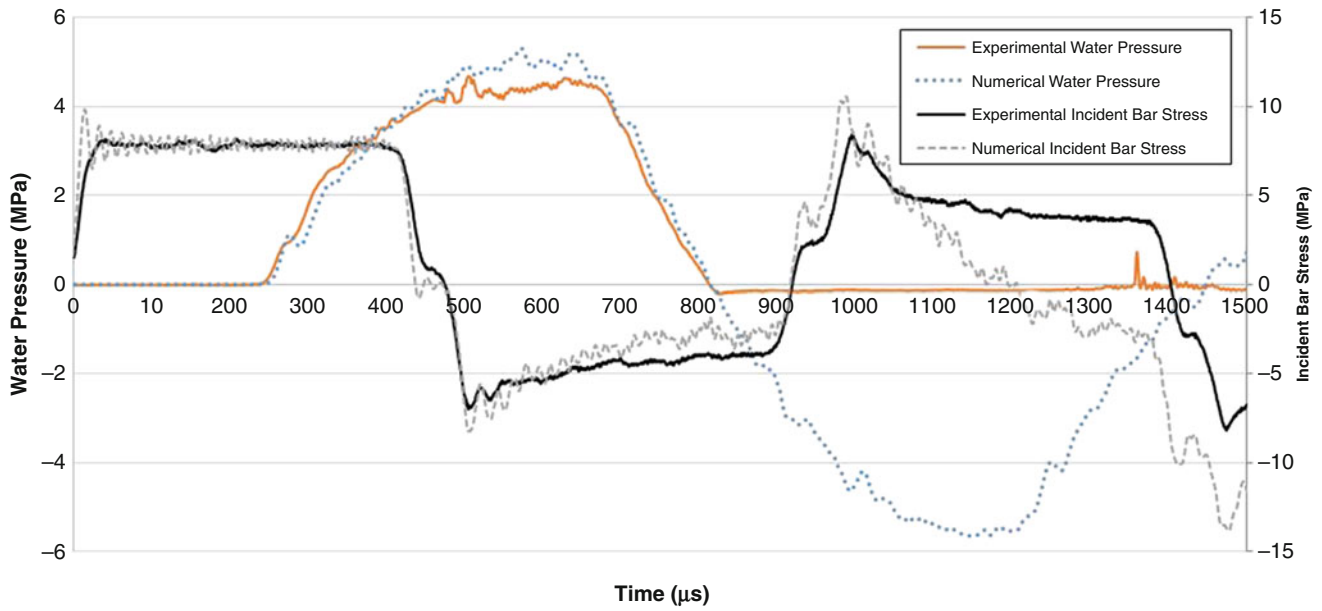
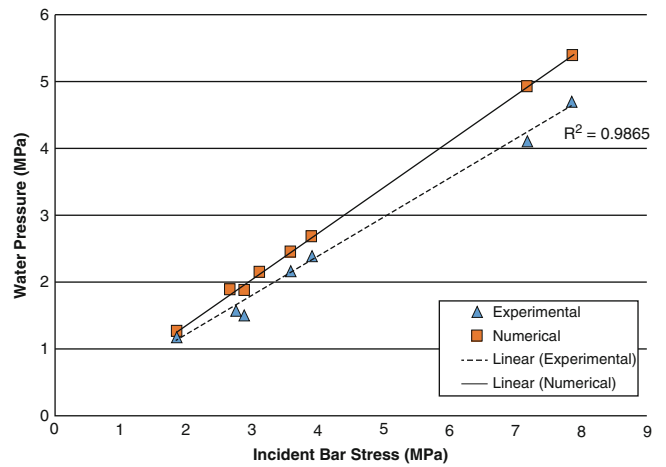


Fig. 8.9 Experimental and numerical water pressure and incident bar stress versus time plot for 1.15 m/s striker velocity

Fig. 8.10 Experimental and numerical data comparison of water pressure versus incident bar stress trends

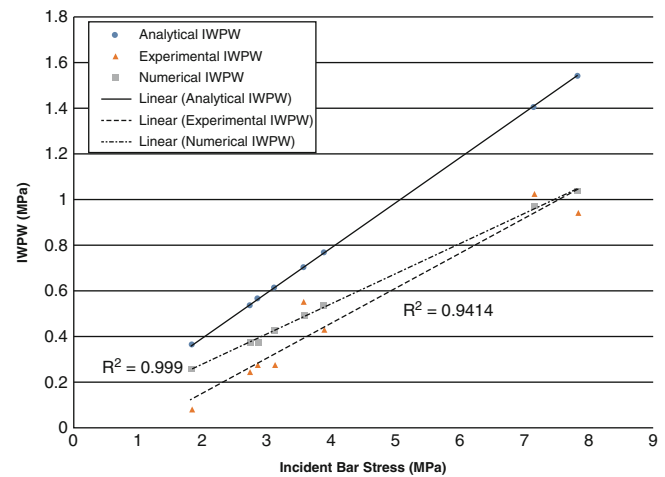


8.4 Discussion and Conclusions

Figure 8.9 shows good agreement between the experimental data and numerical simulation for the 1.15 m/s striker velocity test. There was a small difference between the measured and predicted reflected waves in the bar, attributed to losses in the system due to friction from the o-rings. A small difference was also noted between the measured and simulated positive water pressures that can be attributed to the o-rings sealing the confinement chamber which may decrease the stiffness in the experiment compared to the model. As expected, the negative pressure in the water was not accurately measured for all test cases, due to the inability of the pressure transducer to measure negative pressures. Due to the good agreement of the positive pressures in the water, the maximum negative pressures that can be achieved in the experimental tests can be assumed to be approximately that of the negative pressures predicted by the numerical simulations. Cavitation of the water was not defined in the numerical model, therefore the predicted magnitude of the negative pressure in the model could be larger than that achieved in the experimental test, when it exceeds the cavitation pressure of the actual fluid.

The experimental and numerical trends of peak water pressure versus incident bar stress shown in Fig. 8.10 show good agreement. The lesser slope of the experimental trend can be attributed to the compliance of the experimental setup compared to the numerical model, particularly at higher water pressures. The experimental and numerical trends of

Fig. 8.11 Experimental, numerical, and analytical data comparison of IWPW versus incident bar stress trends



IWPW versus incident bar stress shown in Fig. 8.11 also show good agreement. As expected, the analytical values of IWPW are highest because this analysis assumes one-dimensional wave propagation, unlike the numerical and experimental approaches. Likewise, it is expected that the experimental values would have the lowest IWPW values because of the losses in the system that are not included in the numerical model.

Cavitation was observed for all eight tests performed even with a striker velocity as low as 0.27 m/s, suggesting that for future work a different material should be used for the incident and striker bars. Using a bar material with a lower impedance compared to aluminum will reduce the incident wave generated. Changing the bar material is preferred over reducing the striker velocity because vibrational and frictional effects become more significant at lower velocities.

A traditional CSHPB apparatus was modified into a TSHPB to perform preliminary tests investigating the cavitation properties of distilled water. The apparatus was further developed by removing the transmitter bar and using a single-entry confinement chamber to increase the stiffness of the reflection boundary, as well as mounting a pressure transducer to measure static pressure of the water. Both apparatuses were able to produce cavitation in the distilled water using an initial tensile incident wave. To better reproduce the conditions of blast exposure, the apparatus was again modified to generate an initial compressive incident wave. This current CSHPB apparatus has successfully produced cavitation in the distilled water using a reflected compression wave, and the experimental measurements were in good agreement with numerical simulations for all test cases. It was also suggested that the pressure transducer designed for compression inaccurately measures negative pressure and those obtained in the numerical model are the maximum achievable negative pressures that can occur in the experimental tests. Future work will consider alternate bar materials, and testing of CSF.

Acknowledgment The authors would like to acknowledge the financial and technical support of Defence Research and Development Canada—Suffield.

References

1. Scherer, M.R., Weightman, M.M., Radomski, M.V., Davidson, L.F., McCulloch, K.L.: Returning service members to duty following mild traumatic brain injury: exploring the use of dual-task and multitask assessment methods. *Phys. Ther.* **83**, 1254–1267 (2013)
2. Harrigan, T.P., Roberts, J.C., Ward, E.E., Merkle, A.C.: Correlating tissue response with anatomical location of mTBI using a human head finite element model under simulated blast conditions. In: IFMBE Proceedings, College Park, pp. 18–21 (2010)
3. Rosenfeld, J.V., McFarlane, A.C., Bragge, P., Armonda, R.A., Grimes, J.B., Ling, G.S.: Blast-related traumatic brain injury. *Lancet Neurol.* **12** (9), 882–893 (2013)
4. Schmitt, K.-U., Niederer, P.F., Cronin, D.S., Muser, M.H., Walz, F.: *Trauma Biomechanics*, 4th edn. Springer, Berlin (2014)
5. El Sayed, T., Mota, A., Fraternali, F., Ortiz, M.: Biomechanics of traumatic brain injury. *Comput. Methods Appl. Mech. Eng.* **197**(51–52), 4692–4701 (2008)
6. Bass, C.R., Panzer, M.B., Rafaels, K.A., Wood, G., Shridharani, J., Capehart, B.: Brain injuries from blast. *Ann. Biomed. Eng.* **40**(1), 185–202 (2012)
7. Thiruvengadam, A.: *Handbook of Cavitation Erosion*, Rev. edn. Hydronautics, Laurel (1974)
8. Herbert, E., Balibar, S., Caupin, F.: Cavitation pressure in water. *Phys. Rev. E* **74**(4), 041603 (2006)
9. Bir, C.: Measuring Blast-Related Intracranial Pressure within the Human Head. Final Report, U.S. Army Medical Research and Materiel Command, Award No. W81XWH-09-1-0498. (2011)

10. Singh, D., Cronin, D.S., Haladuick, T.N.: Head and brain response to blast using sagittal and transverse finite element models. *Int. J. Numer. Meth. Bio. Eng.* **30**(4), 470–489 (2013)
11. Panzer, M.B., Myers, B.S., Capehart, B.P., Bass, C.R.: Development of a finite element model for blast brain injury and the effects of CSF cavitation. *Ann. Biomed. Eng.* **40**(7), 1530–1544 (2012)
12. Zhang, L., Makwana, R., Sharma, S.: Brain response to primary blast wave using validated finite element models of human head and advanced combat helmet. *Front. Neurol.* **4**, 88 (2013)
13. Singh, D., Cronin, D.S.: Investigation of cavitation using a modified Hopkinson apparatus. In: *Proceedings of SEM, Greenville* (2014)
14. Hong, Y., Canchi, S., King, M., Lee, S.J., Sarntinoranont, M., Subhash, G.: Development of a test system to study brain tissue damage due to cavitation, pp. 2–3 (2014)
15. Conn, P.M.: *Neuroscience in Medicine*, 2nd edn. Humana, Totowa (2003)
16. Cronin, D.S.: Explicit finite element method applied to impact biomechanics problems. In: *IRCOBI, Krakow* (2011)
17. Kandel, E., Schwartz, J., Thomas, J.: *Principles of Neural Science*, 4th edn. McGraw-Hill Medical, New York (2013)